The Quantum Coherent Mechanism for Singlet Fission: Experiment and Theory

WAI-LUN CHAN,[†] TIMOTHY C. BERKELBACH,[‡]
MAKENZIE R. PROVORSE,[§] NICHOLAS R. MONAHAN,[‡]
JOHN R. TRITSCH,[‖] MARK S. HYBERTSEN,[⊥] DAVID R. REICHMAN,*,[‡]
JIALI GAO,*,[§] AND X.-Y. ZHU*,[‡]

[†]Department of Physics and Astronomy, University of Kansas, Lawrence, Kansas 66045, United States, [‡]Department of Chemistry, Columbia University, New York, New York 10027, United States, [§]Department of Chemistry, University of Minnesota, Minneapolis, Minnesota 55455, United States, [‖]Texas Materials Institute, University of Texas, Austin, Texas 78712, United States, and [⊥]Center for Functional Nanomaterials, Brookhaven National Laboratory, Upton, New York 11973, United States

CONSPECTUS

The absorption of one photon by a semiconductor material usually creates one electron–hole pair. However, this general rule breaks down in a few organic semiconductors, such as pentacene and tetracene, where one photon absorption may result in two electron–hole pairs. This process, where a singlet exciton transforms to two triplet excitons, can have quantum yields as high as 200%. Singlet fission may be useful to solar cell technologies to increase the power conversion efficiency beyond the so-called Shockley-Queisser limit. Through time-resolved two-photon photoemission (TR-2PPE) spectroscopy in crystalline pentacene and tetracene, our lab has recently provided the first spectroscopic signatures in singlet fission of a critical intermediate known as the multiexciton state (also called a correlated triplet pair). More importantly, we found that population of the multiexciton state rises at the same time as the singlet state on the ultrafast time scale upon photoexcitation. This observation does not fit with the traditional view of singlet fission involving the incoherent conversion of a singlet to a triplet pair. However, it provides an experimental foundation for a quantum coherent mechanism in which the electronic coupling creates a quantum superposition of the singlet and the multiexciton state immediately after optical excitation.

In this Account, we review key experimental findings from TR-2PPE experiments and present a theoretical analysis of the quantum coherent mechanism based on electronic structural and density matrix calculations for crystalline tetracene lattices. Using multistate density functional theory, we find that the direct electronic coupling between singlet and multiexciton states is too weak to explain the experimental observation. Instead, indirect coupling via charge transfer intermediate states is two orders of magnitude stronger, and dominates the dynamics for ultrafast multiexciton formation. Density matrix calculation for the crystalline tetracene lattice satisfactorily accounts for the experimental observations. It also reveals the critical roles of the charge transfer states and the high dephasing rates in ensuring the ultrafast formation of multiexciton states. In addition, we address the origins of microscopic relaxation and dephasing rates, and adopt these rates in a quantum master equation description. We show the need to take the theoretical effort one step further in the near future by combining high-level electronic structure calculations with accurate quantum relaxation dynamics for large systems.
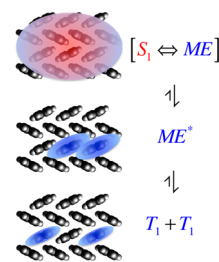
1. Introduction

Since its discovery in 1965,[1] singlet fission, that is, the conversion of a singlet exciton into two triplet excitons in molecular materials, has remained a fascinating but exotic photophysical phenomenon.[2] Recently, renewed interest in singlet fission[3] has been driven mainly by the potential application of this process in boosting the power conversion efficiency of solar cells.[4,5] Singlet fission has been reported for a number of molecular systems. Particularly noteworthy are crystalline solids or aggregates of tetracene,[6,7] pentacene,[8,9] 1,3-diphenylisobenzofuran,[10] and carotenoids[11] where high singlet fission yields have been reported.

The predominant mechanism used to describe singlet fission comes from Merrifield's theory[12,13] for the reverse

process of triplet−triplet annihilation and can be written as

$$S_1 \underset{k_2}{\overset{k_{-2}}{\rightleftharpoons}} {}^1(TT) \underset{k_1}{\overset{k_{-1}}{\rightleftharpoons}} T_1 + T_1 \qquad (1)$$
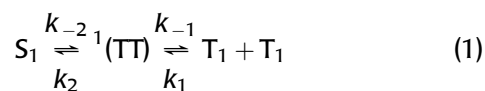
where a photoexcited singlet (S_1) evolves into two triplets on adjacent chromophores known as a correlated triplet pair, ${}^1(TT)$, or a multiexciton state (ME), which further separates into two individual triplets (T_1). The intermediate ${}^1(TT)$ state, proposed first as a nonradiative decay mechanism in crystalline tetracene,[14] is a coherent superposition of the nine triplet pair states.[13,15] Coherent oscillations between different spin states of ${}^1(TT)$ have been observed on the nanosecond time scale in fluorescence from tetracene.[16] Unlike long-time spin dynamics, much less is known about how ME is formed from S_1, which is determined by the electronic Hamiltonian and happening on the shorter time scale of femtoseconds to picoseconds. Earlier treatments[2,3] assumed an incoherent rate constant (k_{-2}) for the $S_1 \rightarrow$ ME transition. Zimmerman and co-workers attributed conical intersections as responsible for the ultrafast transition from S_1 to ME in pentacene.[17,18] Greyson et al.[19] and Teichen and Eaves[20] studied the $S_1 \rightarrow$ ME transition via intermediate charge transfer (CT) states.

Despite the progress described above, the lack of experimental observation of ME has been a major obstacle to establishing the singlet fission mechanism.[3] Previous time-resolved studies of singlet fission have relied on transient absorption and time-resolved fluorescence spectroscopies. There is now a consensus that singlet fission occurs on the ultrafast time scale of 70−100 fs in crystalline pentacene.[8,9] In crystalline tetracene, the reported singlet fission times vary broadly, from less than 300 fs to about 1 ns,[3] although recent measurements seem to converge to the time scales of 50−80 ps based on population decay of S_1.[7] There has been no experimental observation of ME until recently when Zhu and co-workers[21,22] applied time-resolved two-photon photoemission spectroscopy (TR-2PPE) to tackle the problem, as detailed below.

2. Experimental Evidence for the Multiexciton State and a Quantum Coherent Mechanism

In TR-2PPE, a pump laser pulse creates excitonic state(s); after a controlled time-delay, the probe pulse ionizes the excitonic states and the photoelectrons are detected. For ME, photoionization destroys the correlated triplet pair by
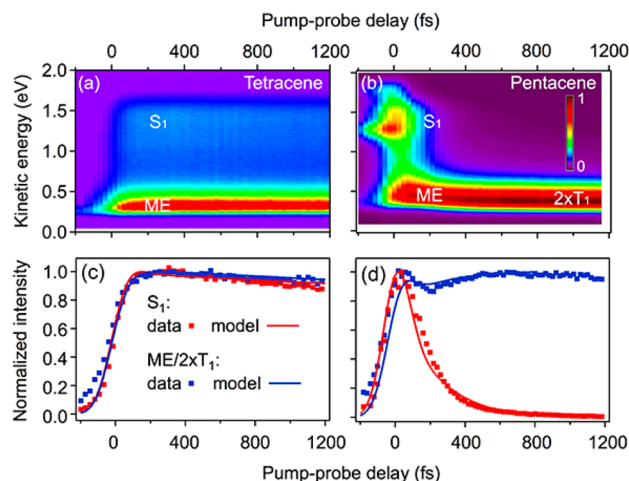

FIGURE 1. Pseudocolor plots of TR-2PPE spectra of tetracene (a) and pentacene (b) thin films,[21,22] excited at $h\nu_1 = 2.32$ and 2.15 eV, respectively. The excitonic states are probed with an ionization photon of $h\nu_2 = 4.65$ eV. The energetic positions of the S_1, ME, and $2 \times T_1$ are indicated. The lower panels show the normalized 2PPE intensities of the S_1 (red dots) and the ME/$2 \times T_1$ (blue dots) states for tetracene (c) and pentacene (d), respectively. The solid curves are simulations from the three-state model.

ionizing one triplet, leaving behind another triplet and a hole. As a result, ME shows up in a TR-2PPE spectrum with an electron kinetic energy similar to that from an individual T_1, not S_1.

Figure 1a and b shows pseudocolor plots of TR-2PPE spectra for tetracene (a) and pentacene (b) thin films.[21,22] There is a high-energy feature assigned to S_1 and a lower one to T_1. While the formation of S_1 upon photoexcitation and T_1 at longer times are expected, what is most surprising is the observation of a state at nearly the same energy and intensity as T_1 but which rises concurrently with S_1. We assign this T_1-like state at early times to the ME state. The concurrent rise of the S_1 and ME populations cannot be explained by conventional models in which the S_1 converts incoherently to ME, but can be explained by the scheme illustrated below:

$$[S_1 \leftrightarrow ME] \rightleftharpoons ME' \rightleftharpoons T_1 + T_1 \qquad (2)$$
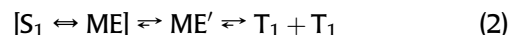
Here, the S_1 state is optically excited and the dark ME state is populated through electronic coupling to S_1, forming a quantum superposition state $[S_1 \leftrightarrow ME]$ on the ultrafast time scale (with a time constant inversely proportional to the coupling strength). Once the ME loses electronic coupling to S_1, we call the resulting multiexciton state ME', which may be initially on a pair of neighboring molecules and may diffuse apart and also loses spin coherence, evolving eventually into two independent

triplets. We define the fission rate as the rate at which the multiexciton state loses electronic coupling to S_1.[22] Note that $[S_1 \leftrightarrow ME]$ can be said to possess "state coherence", not "process coherence" resulting, for example, from the excitation of multiple bright states within the bandwidth of a short laser pulse.[23]

The TR-2PPE results show a clear difference between pentacene and tetracene. In pentacene, the $[S_1 \leftrightarrow ME]$ state is short-lived ($\tau_{SF} = 100 \pm 20$ fs), and this can be attributed to relaxation processes that destroy the quantum coherence on an ultrafast time scale. The energetic relaxation is characterized by a total decrease of 0.11 eV in electron energy from the multiexciton state, seen in Figure 1b, as predicted by quantum chemistry calculations.[17] In tetracene, the $[S_1 \leftrightarrow ME]$ superposition state is much longer-lived ($\tau_{SF} = 7$ ps), Figure 1c,[22] and this time scale has also been verified in analysis of one versus two electron transfer from the superposition state.[24] There is no measurable energetic relaxation as the ME state evolves into $ME'/2T_1$ (Figure 1a). The definition of singlet fission time based on the lifetime of $[S_1 \leftrightarrow ME]$ is different than traditional definitions based on the S_1 population decay time of $\sim 60-80$ ps.[7,22]

To model the excitation and the subsequent evolution of the superposition state, we start with a phenomenological three-state model, where the Hamiltonian of the system can be written as

$$\hat{H}_{ME} = \begin{pmatrix} E_{S0} & -\mu E(t) & 0 \\ -\mu E(t) & E_{S1} & -W \\ 0 & -W & E_{ME} \end{pmatrix} \qquad (3)$$

where E_{S0}, E_{S1}, E_{ME} are the energies of the S_0 (ground state), S_1, and ME state,s respectively. The S_1 state is populated from S_0 by the laser field $\mu E(t)$ in the dipole approximation and converts coherently to the dark ME state through the electronic coupling W. We obtain the time evolution of the states by a density matrix approach using the Liouville−von Neumann equation,[25]

$$i\hbar \frac{\partial \hat{\rho}}{\partial t} = [\hat{H}_{ME}, \hat{\rho}] - i\hbar \hat{D} \qquad (4)$$

where the diagonal ρ_{ii} element represents the population of state i; the off-diagonal ρ_{ij} represents the coherence between states i and j; and $D_{ij} = \Gamma_{ij}(\rho_{ij} - \rho^0_{ij})$ characterizes the interaction with the environment. The diagonal elements of Γ_{ij} are population relaxation rates while the off-diagonal elements are coherence dephasing rates.[21] ρ^0 is the steady-state density matrix, for which we assume all off-diagonal terms are zero. To account for

the experimental observation, we find that W must be of the order of 10^2 meV, as shown by solid curves in Figure 1c and d for $W = 200$ and 330 meV, respectively, along with normalized experimental data.

The experimental observation and phenomenological simulation in Figure 1 suggest strong electronic coupling between S_1 and ME. This raises a number of interesting questions: (1) Is there a theoretical basis for the large coupling constant between S_1 and ME? (2) Is the microscopic origin of this coupling direct or involving charge-transfer intermediates?[19] (3) How does delocalization in the crystalline solid affect singlet-multiexciton coupling? (4) What is the role of coupling to the thermal bath in singlet fission dynamics? In the following, we present our initial theoretical effects in addressing the above questions.[26,27,28]

3. Multistate Density Functional Theory: Indirect Coupling Between S_1 and ME via CT States

We start by answering the first two questions, that is, the magnitude and the direct or indirect nature of S_1-ME coupling. It is difficult if not impossible to determine the intermolecular electronic coupling directly using conventional wave functional theory or density functional theory (DFT) because molecular or Kohn−Sham orbitals are delocalized over the entire system. Here, we employ multistate density functional theory (MSDFT),[29] in which the exciton and CT wave functions of each monomer are localized within the molecular fragment, to quantify the energies of S_1, ME, and CT states and the electronic coupling matrix elements.[26] In a crystalline solid, S_1 is delocalized due to dipole−dipole interactions, forming a Frenkel exciton band, while CT excitons are delocalized due to both electronic and dipole−dipole interactions.

Our calculations employed a tetracene monolayer based on the crystal structure in the $a-b$ plane for a tetracene thin-film,[30] Figure 2, consisting of 56 (7 × 8) monomers with a subset (gold color) treated quantum mechanically. In MSDFT,[29] each monomer is treated by DFT with Kohn−Sham orbitals strictly localized within the monomer space, that is, block-localized Kohn−Sham (BLKS) orbitals expanded over basis functions located on the monomer atoms only. The monolayer wave function is approximated by a Hartree product of the determinant wave functions of individual monomers. Consequently, Coulomb and mutual polarization interactions among all monomers are explicitly included. To account for the exchange interaction between two molecules that form each ME or CT state, the interacting
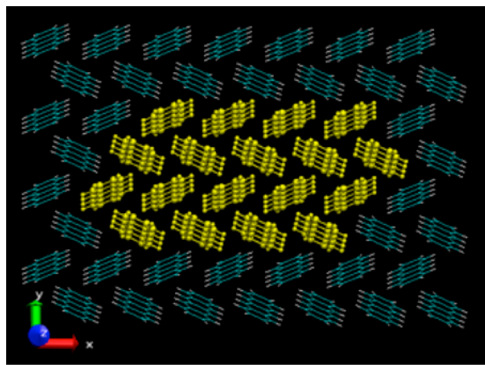
FIGURE 2. Structure of the tetracene monolayer containing 56 molecules, with the gold color region treated quantum mechanically.

monomers are grouped into a single fragment, described by a Slater determinant that is constructed from the monomeric BLKS orbitals. Thus, the Kohn–Sham functions for the S_1 state localized on monomer u, the triplet pair with an overall singlet spin (ME), and the CT state involving monomers u and v, are given:[26]

$$\Phi_{uv}(S_1) = \hat{A}\{\Omega_u(S_1)\Omega_v(S_0)\} \prod_{k \neq u,v}^{N} \Psi_k(S_0) \quad (5a)$$

$$\Phi_{uv}(ME) = \hat{A}\{\Omega_u(T_1^{\uparrow\uparrow})\Omega_v(T_1^{\downarrow\downarrow})\} \prod_{k \neq u,v}^{N} \Psi_k(S_0) \quad (5b)$$

$$\Phi_{uv}(CT) = \hat{A}\{\Omega_u(D^{\bullet+})\Omega_v(A^{\bullet-})\} \prod_{k \neq u,v}^{N} \Psi_k(S_0) \quad (5c)$$

where N is the total number of tetracene molecules in the system, $\hat{A}$ is the antisymmetrizer, and Ω_u denotes the product of occupied BLKS orbitals on monomer u. In eq 5, $\Psi_k(S_0)$ is a Slater determinant of monomer k in the ground state, and $\hat{A}\{\Omega_u(X)\ \Omega_v(Y)\}$ specifies a superfragment consisting of two coupled monomers u and v, in which the corresponding localized electronic configurations are specified in parentheses with $X = S_0, S_1, T_1, D^{\bullet+}$, and $A^{\bullet-}$; the last two represent molecular donor and acceptor, respectively, in the CT state. The arrows in $T_1^{\uparrow\uparrow}$ and $T_1^{\downarrow\downarrow}$ are used to emphasize that S_z of the coupled triplet configurations is zero. For the coupled monomer pair in $\hat{A}\{\Omega_u(X)\ \Omega_v(Y)\}$, both Coulomb and exchange interactions are explicitly treated by DFT with BLKS orbitals, whereas only the Coulomb potential from the rest of the system is included.[26]

We performed all calculations in DFT with the PBE0 functional and the 6-31G(d) basis set,[31,32] using a modified version of GAMESS,[33] as detailed elsewhere[26] and summarized in the Supporting Information. The intermolecular electronic coupling constants, directly expressed in $\langle\Phi_{uv}(S_1)|\hat{H}|\Phi_{uv}(ME)\rangle$ or mediated through CT, $\langle\Phi_{uv}(S_1)|\hat{H}|\Phi_{uv}(CT)\rangle$ and $\langle\Phi_{uv}(CT)|\hat{H}|\Phi_{uv}(ME)\rangle$, were determined by MSDFT.[26,29] Table S1 (Supporting Information) lists the computed electronic couplings between various states in different dimer pairs. The direct coupling between S_1 and ME and between two ME states by the two-electron part of the Hamiltonian is rather weak, in the range of 0.5–3 meV for the nearest tetracene neighbors. For comparison, a value of ~5 meV was obtained for a pentacene dimer by a restricted active space and two spin flip method (RAS(4,4)-2SF).[18] Note that the strong S_1–S_1 electronic coupling (3 to 65 meV) is responsible for the formation of a Frenkel exciton band and, along with the significant S_1–CT coupling, for the Davydov splitting in tetracene.[34]

The most significant finding is that electronic coupling constants between S_1 and CT states or between ME and CT states (50–140 meV, Table S2) are 1–2 orders of magnitude larger than those between S_1 and ME. Thus, the large S_1–ME coupling suggested in Figure 1 is most likely *not* due to direct coupling, but a result of indirect coupling via the CT intermediate states.

4. Density Matrix Dynamics: Role of Delocalization and the Thermal Bath

We now demonstrate using density matrix theory that the calculated coupling matrix elements from section 3 can indeed account for salient features in experimental observations. In particular, we address the roles of delocalization and coupling to the thermal bath (i.e., questions 3 and 4 at the end of section 2) by calculating the time evolution of the S_1, CT, and ME populations for a crystalline tetracene lattice in a thermal bath at both phenomenological and microscopic levels.

We start with solving eq 4 using experimental energy detuning values of $E_{ME} - E_{S1} = 0.17$ eV, $E_{CT} - E_{S1} = 0.3$ eV,[22,34] and calculated matrix elements for tetracene clusters of various sizes. As an example, the Hamiltonian for a five-molecule cluster is shown schematically in Figure 3 and detailed in the Supporting Information. This Hamiltonian, which is not spin-adapted, includes a total of 10 S_1 states, 16 ME states, and 32 CT states. Here, we included only nearest neighbors except monomers 3 and 5 (Figure 3a and Table S1). Given the large size of the system, we first adopt a phenomenological description of relaxation and dephasing rates. Since we focus on the initial excitation of the
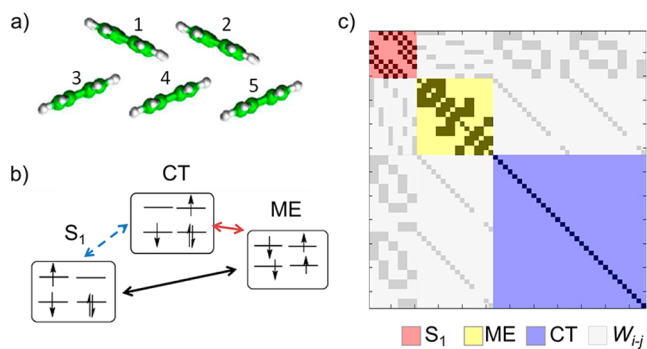
FIGURE 3. (a) Schematic illustration of a five molecule cluster used in density matrix modeling; (b) coupling of S_1 with ME directly (black arrow) or via CT exciton intermediates (blue and red arrows); (c) graphical illustration of the Hamiltonian containing three diagonal blocks: S1 (pink, 10 states), ME (yellow, 16 states), and CT (violet, 32 states). The nonzero elements are shown as dark spots. The gray regions show coupling constants between different types of states, with nonzero coupling constants in dark gray.
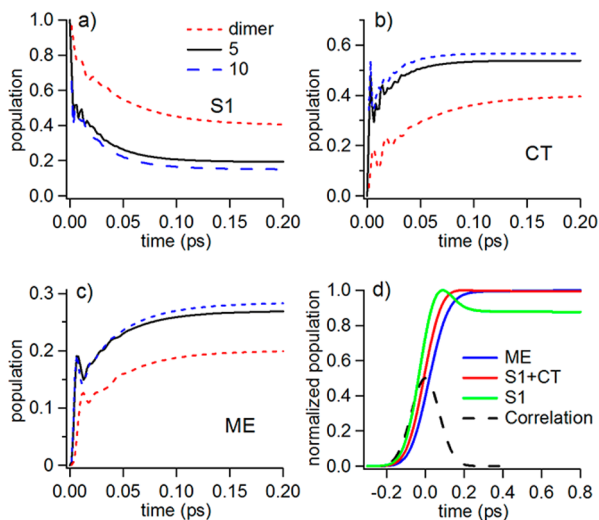

FIGURE 4. Populations of the S1 (a), CT (b), and ME (c) states as a function of time after photoexcitation obtained from density matrix calculation of crystalline tetracene. We show the results for three cluster sizes (red, black, and blue for 2, 5, and 10 tetracene molecules). Panel (d) shows the S1 + CT and ME population for the 5 tetracene cluster, convoluted with a Gaussian function with a fwhm of 170 fs to represent the experimental cross-correlation.

superposition state, in particular, the fast rise in ME population, we set all population decay rates (Γ_{ii}) to zero and set all dephasing rates (Γ_{ij}) to 50 meV/$\hbar$, which is typical for electronic dephasing rates in molecules; we will return to these issues below when we present preliminary results of a microscopic Redfield theory calculation that includes both population decay and coherence dephasing. At $t = 0$, we assume the singlet population is distributed uniformly over the molecules in the cluster, with the sum of amplitudes equaling one, since S_1 is known to delocalize over
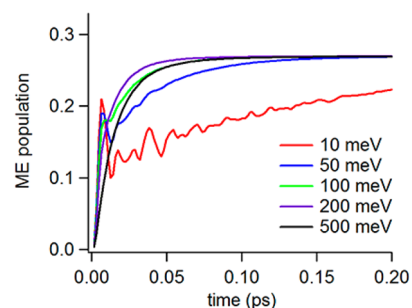

FIGURE 5. Calculated time-dependent population of the ME state for a cluster size of five tetracene molecules in the crystalline lattice at the indicated dephasing rates (10 − 500 meV).

approximately 10 molecules in crystalline tetracene.[7] We evolve the density matrix $\rho(t)$ using eq 4.

Figure 4a−c shows S_1, CT, and ME populations for cluster sizes of 2, 5, and 10 tetracene molecules, respectively, embedded electrostatically in the monolayer environment depicted in Figure 2. For all sizes, S_1 converts to CT and ME within the first 200 fs, after which the dephasing inhibits any further population transfer. The rise times for the CT and ME populations for a dimer are slightly longer than those of larger tetracene clusters. As the cluster size increases, the S_1 state on each molecule can couple to multiple CT and ME states, proportional to the number of nearest neighbors; this increases the number of channels for the conversion from S_1 to CT and ME, and hence the conversion rate. A similar density-of-states argument has been proposed for multiexciton generation in semiconductor quantum dots.[35]

The S_1, S_1 + CT, and ME populations from the simulation (for a cluster of five) are convoluted with the experimental two-pulse cross-correlation and shown in Figure 4d. The S_1 + CT and ME populations rise up with a time-lag of only ∼20 fs, and the two populations maintain a constant ratio after excitation, in qualitative agreement with experimental observation in Figure 1. As a control, we have also run simulation with the initial excitation on CT and find nearly identical results as those in Figure 4d.

Figure 5 shows the rise of the ME population calculated with different electronic dephasing rates Γ_{ij}. The nearly instantaneous rise time of ME depends solely on the value of the electronic couplings W_{ij} whereas the longer time dynamics are determined by the dephasing rate. For a smaller $\hbar\Gamma_{ij}$ (10 meV), we see a weaker damping of the coherent oscillation. In the case of tetracene, singlet fission is an endothermic process with both E_{ME} and E_{CT} higher than E_{S1}; as the population of CT and ME states increases, the total energy of the electronic subsystem changes. In eq 4, this energy change is accomplished through coupling to the environment via the dephasing term Γ_{ij}. For small Γ_{ij}, the

rise time of ME population is limited by the slow energy exchange between the system and the environment. For larger Γ_{ij}, the dephasing process becomes approximately resonant with the electronic transitions and the rise time is determined only by the electronic coupling constants.

We now consider the microscopic origins of the dephasing rates and rigorously derive the density matrix dynamics in eq 4 using techniques from quantum relaxation theory. Specifically, the density matrix ρ should be understood as the *reduced* density matrix obtained by averaging over microscopic environmental degrees of freedom. This statistical reduction is the physical origin for the phenomenological dephasing and relaxation processes. In this approach, one begins with an extended Hamiltonian,

$$\hat{H} = \hat{H}_{ME} + \hat{H}_B + \hat{H}_{ME-B} \tag{6}$$

which comprises the electronic, the environmental bath, and the interaction between the two. Under the assumption of bilinear coupling to a bath of phonons,[27] the effects of the environment can be completely characterized by the so-called spectral density,

$$J_i(\omega) = \frac{\pi}{2} \sum_k \frac{c_{k,i}^2}{\omega_k} \delta(\omega - \omega_k) \tag{7}$$

where $c_{k,i}$ quantifies the coupling between energy level i and the phonon mode with frequency ω_k. For conjugated organic chromophores, like tetracene and pentacene, the spectral density is peaked at the well-known vibronic progression frequency of ~ 1450 cm^{-1}.[34] The quantitative structure of $J(\omega)$ can be determined by a combination of classical molecular dynamics and quantum chemistry calculations,[36] which can be used to parametrize common functional forms of the spectral density.

By performing a dynamical perturbation theory to second order in the electron−phonon interaction, and employing the secular and Markov approximations, one arrives at the well-known Redfield theory equation of motion,[37,38]

$$i\hbar \frac{\partial \hat{\rho}}{\partial t} = [\hat{H}_{ME}, \hat{\rho}] - i\hbar \hat{R}\hat{\rho} \tag{8}$$

The Redfield tensor is a four-index quantity, $\hat{R}_{ijkl}$, describing population relaxation and coherence dephasing induced by the environment at temperature T, and can be shown to produce a Boltzmann-distributed steady-state reduced density matrix,

$$\hat{\rho}(t \rightarrow \infty) = \hat{\rho}_0 = Z_{ME}^{-1} \exp(-\hat{H}_{ME}/k_B T) \tag{9}$$

While the Redfield theory equation of motion takes the same general form as eq 4, the rates composing the Redfield tensor $\hat{R}$ have explicit microscopic expressions depending on both the system and bath degrees of freedom. These expressions, in addition to being unbiased and more general than phenomenological constants, can also provide valuable physical insight. For example, the population relaxation elements, in the electronic eigenstate basis that diagonalizes $\hat{H}_{ME}$, are given by the expressions

$$R_{\alpha\alpha\beta\beta} = C_{\alpha\beta} J(\omega_{\alpha\beta}) n_{BE}(\omega_{\alpha\beta})$$
$$R_{\beta\beta\alpha\alpha} = C_{\alpha\beta} J(\omega_{\alpha\beta})[n_{BE}(\omega_{\alpha\beta}) + 1] \tag{10}$$

where $\omega_{\alpha\beta} = (E_\alpha - E_\beta)/\hbar$ is assumed positive, $C_{\alpha\beta}$ is a constant determined by the diagonalizing transformation, and $n_{BE}(\omega) = [\exp(\hbar\omega/k_B T) - 1]^{-1}$ is the Bose−Einstein distribution. Equation 10 demonstrates that the population transfer rate between two states is proportional to the density of phonon modes at their energy difference and the probability that those modes are thermally occupied. Physically, the electronic subsystem is thermalized by the absorption and emission of phonons.

The use of constant, uniform dephasing rates in the previous section is somewhat akin to an infinite temperature assumption, and thus the population dynamics overestimate the effects of entropy. Although such an analysis sheds light on the important role entropy can play when transitioning from molecular dimers to bulk materials, ultimately the finite-temperature formalism presented above should be preferred as it correctly interpolates between the energetically and entropically dominated regimes, guaranteeing a steady-state Boltzmann distribution. When such finite-temperature rates are used, we have shown in pentacene that a CT-mediated superexchange mechanism becomes a viable singlet fission pathway.[28] In this regime, the electronic excitation quantum mechanically tunnels through *virtual* CT states in passing from S_1 to ME. Our superexchange result is robust even in the presence of very high CT state energies.

To demonstrate this formalism, we consider a simple three-state model Hamiltonian comprising the S_1, CT, and ME states for a pentacene dimer. We neglect the direct S_1 to ME coupling and choose the remaining coupling values $W_{S1-CT} = W_{CT-ME} = 50$ meV, in accord with the calculations presented in section 3. The energy detuning values are
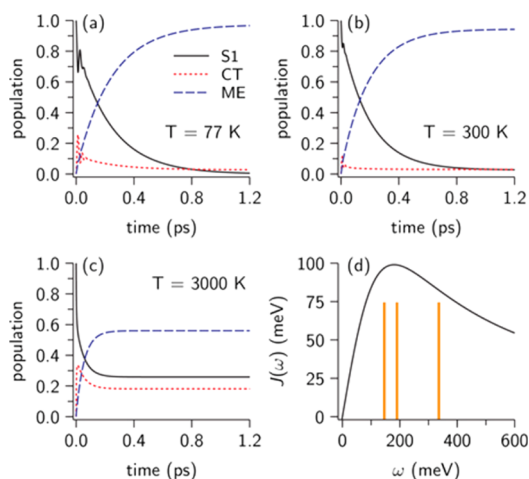
FIGURE 6. Population dynamics of the S1, CT, and ME states as calculated by the Redfield quantum master equation for a pentacene dimer. Dynamics are calculated at the three temperatures indicated in panels (a)–(c). Panel (d) shows the bath spectral density employed along with the three transition energy differences of the electronic Hamiltonian.

chosen to be representative of a pentacene dimer, $E_{S1} - E_{TT} = 200$ meV and $E_{CT} - E_{TT} = 300$ meV.[17,18,27,34] In Figure 6, we show the population dynamics of the three states as calculated by the Redfield master equation, for an initially excited S_1 state. Overall, we see that highly efficient fission occurs in 100 fs and the negligible CT population in panels (a) and (b) is characteristic of a superexchange mechanism proceeding through virtual CT states.[27,28] As explained above, the relaxation rates are largely determined by the spectral density, which we take to be of the ohmic form, $J(\omega) = 2\lambda\Omega\omega/(\omega^2 + \Omega^2)$, with reorganization energy $\lambda = 100$ meV and characteristic bath frequency $\hbar\Omega = 180$ meV (1450 cm^{-1}). In Figure 6d, we plot the spectral density along with the three electronic eigenvalue energy differences, showing the strong overlap, which means that there are many available phonons to supply or remove the required excess energy. The additional temperature dependence of the rates is depicted in panels (a)–(c), showing that the fission is largely temperature independent until very high temperatures, at which point the rate increases and the steady state population becomes more equally distributed. Such temperature-dependent studies are clearly only accessible via a master equation whose rates obey detailed balance, eq 10.

The ~100 fs rise time for the ME population calculated above from the master equation is longer than the ≤20 fs time determined from 2PPE experiments in Figure 1b and d. One limitation of the calculation may be attributed to the reduced density-of-states of a dimer; work is currently underway to extend this treatment to larger clusters and crystals. Another possibility may be the approximate nature of equating photoemission intensities to state populations. As another future research direction, we plan to extend our density matrix dynamics to include the photo-ionization step for a more direct comparison with TR-2PPE experiments.

5. Summary

We present our understanding of singlet fission dynamics in organic semiconductors. Recent measurements by time-resolved two-photon photoemission spectroscopy in crystalline pentacene and tetracene have provided an experimental foundation for the quantum coherent mechanism in singlet fission. However, calculations based on multistate density functional theory showed that the direct electronic coupling between singlet and multiexciton states is too weak to explain the ultrafast formation of multiexciton states observed in experiment. Instead, indirect coupling via charge transfer intermediate states are 2 orders of magnitude stronger. Density matrix modeling with the calculated coupling matrix elements involving singlet, charge transfer, and multiexciton states for the crystalline tetracene lattice satisfactorily accounts for the experimental observation. This modeling reveals the critical roles of the intermediate charge transfer states, the high density of states in the multiexciton manifold, and the environmental dephasing processes in ensuring the ultrafast formation of multiexciton states. We address the origins of microscopic relaxation and dephasing rates and adopt such rates in a quantum master equation description, which yields encouraging results that are in qualitative agreements with experimental findings on singlet fission. These successful approaches motivate us to take the theoretical effort one step further in the near future by marrying high-level electronic structure calculations with accurate quantum relaxation dynamics for realistic system sizes.

Supporting Information. Density matrix formulism for tetracene cluster; additional notes on the simulations of the coupling energies. This material is available free of charge via the Internet at http://pubs.acs.org.

BIOGRAPHICAL INFORMATION

Wai-Lun Chan earned his Ph.D. from Brown University in 2007 and did postdoctoral research at the University of Illinois at Urbana—Champaign and the University of Texas at Austin. He is now an assistant professor of Physics at University of Kansas.

Timothy C. Berkelbach received his B.A. in chemistry and physics from New York University in 2009. He is pursuing his Ph.D. in chemical physics in the Reichman group at Columbia University.

Makenzie R. Provorse received her B.S. in chemistry at Kansas State University in 2009. She is currently pursuing her Ph.D. in the Gao group at the University of Minnesota.

Nicholas R. Monahan received a B.S. (2009) and a M.S. (2010) with first class honors from Victoria University in New Zealand. He is pursuing his Ph.D. in the Zhu group on a Fulbright-New Zealand Ministry of Science and Innovation Graduate Award.

John R. Tritsch received his B.S. in chemistry (2009) from the University of Wisconsin—Eau Claire. He is currently pursuing his Ph.D. in the Zhu group at the University of Texas at Austin.

Mark S. Hybertsen received a Ph.D. in Physics from University of California at Berkeley (1986). Following appointments at Bell Laboratories and Columbia University, he is now leading the Theory and Computation Group in the Center for Functional Nanomaterials at Brookhaven National Laboratory.

David R. Reichman is a Professor of Chemistry at Columbia University. Before joining the Columbia faculty, he was a professor at Harvard University. His group focuses on the theoretical description of quantum and classical phenomena in novel materials and condensed phases.

Jiali Gao is a Professor of Chemistry at the University of Minnesota. His research interests include computational biophysics and chemistry.

X.-Y. Zhu is a Professor of Chemistry at Columbia University. He is interested in photophysics and solar energy conversion, with a particular focus on organic semiconductors and nanomaterials.

FOOTNOTES

*To whom correspondence should be addressed. E-mail: xyzhu@columbia.edu (X.-Y.Z.); gao@jialigao.org (J.G.); drr2103@columbia.edu (D.R.R.).
The authors declare no competing financial interest.

REFERENCES

1 Singh, S.; Jones, W. J.; Siebrand, W.; Stoicheff, B. P.; Schneider, W. G. Laser Generation of Excitons and Fluorescence in Anthracene Crystals. *J. Chem. Phys.* **1965**, *42*, 330–340.

2 Pope, M.; Swenberg, C. F. *Electronic Processes in Organic Crystals and Polymers*, 2nd ed.; Oxford University Press: New York, 1999; pp 1—1328.

3 Smith, M. B.; Michl, J. Singlet fission. *Chem. Rev.* **2010**, *110*, 6891–6936.

4 Hanna, M. C.; Nozik, A. J. Solar conversion efficiency of photovoltaic and photoelectrolysis cells with carrier multiplication absorbers. *J. Appl. Phys.* **2006**, *100*, 074510.

5 Paci, I.; Johnson, J. C.; Chen, X. D.; Rana, G.; Popović, D.; David, D. E.; Nozik, A. J.; Ratner, M. A.; Michl, J. Singlet fission for dye-sensitized solar cells: can a suitable sensitizer be found? *J. Am. Chem. Soc* **2006**, *128*, 16546–16553.

6 Kazzaz, A. A.; Zahlan, A. B. Temperature Dependence of Crystalline Tetracene Fluorescence. *J. Phys. Chem.* **1968**, *48*, 1242–1245.

7 Burdett, J. J.; Müller, A. M.; Gosztola, D.; Bardeen, C. J. Excited state dynamics in solid and monomeric tetracene: The roles of superradiance and exciton fission. *J. Chem. Phys.* **2010**, *133*, 144506.

8 Jundt, C.; Klien, G.; Sipp, B.; Le Moigne, J.; Joucla, M.; Villaeys, A. A. Exciton dynamics in pentacene thin films studied by pump-probe spectroscopy. *Chem. Phys. Lett.* **1995**, *241*, 84–88.

9 Rao, A.; Wilson, M. W. B.; Hodgkiss, J. M.; Albert-Seifrid, S.; Bässler, H.; Friend, R. H. Exciton fission and charge generation via triplet excitons in pentacene/C_{60} bilayers. *J. Am. Chem. Soc.* **2010**, *132*, 12698–12703.

10 Johnson, J. C.; Nozik, A. J.; Michl, J. High triplet yield from singlet fission in a thin film of 1,3-diphenylisobenzofuran. *J. Am. Chem. Soc.* **2010**, *132*, 16302–16303.

11 Wang, C.; Tauber, M. J. High-yield singlet fission in a zeaxanthin aggregate observed by picosecond resonance raman spectroscopy. *J. Am. Chem. Soc.* **2010**, *132*, 13988–13991.

12 Merrifield, R. E. Theory of Magnetic Field Effects on the Mutual Annihilation of Triplet Excitons. *J. Chem. Phys.* **1968**, *48*, 4318–4318.

13 Johnson, R.; Merrifield, R. Effects of Magnetic Fields on the Mutual Annihilation of Triplet Excitons in Anthracene Crystals. *Phys. Rev. B* **1970**, *1*, 896–902.

14 Swenberg, C. E.; Stacy, W. T. Bimolecular radiationless transitions in crystalline tetracene. *Chem. Phys. Lett.* **1968**, *2*, 327–328.

15 Geacintov, N.; Pope, M.; Vogel, F. Effect of Magnetic Field on the Fluorescence of Tetracene Crystals: Exciton Fission. *Phys. Rev. Lett.* **1969**, *22*, 593–596.

16 Burdett, J. J.; Bardeen, C. J. Quantum Beats in Crystalline Tetracene Delayed Fluorescence Due to Triplet Pair Coherences Produced by Direct Singlet Fission. *J. Am. Chem. Soc.* **2012**, *134*, 8597.

17 Zimmerman, P. M.; Zhang, Z.; Musgrave, C. B. Singlet fission in pentacene through multi-exciton quantum states. *Nat. Chem.* **2010**, *2*, 648–652.

18 Zimmerman, P. M.; Bell, F.; Casanova, D.; Head-Gordon, M. Mechanism for Singlet fission in Pentacene and Tetracene: From Single Exciton to Two Triplets. *J. Am. Chem. Soc.* **2011**, *133*, 19944–19952.

19 Greyson, E. C.; Vura-Weis, J.; Michl, J.; Ratner, M. A. Maximizing singlet fission in organic dimers: theoretical investigation of triplet yield in the regime of localized excitation and fast coherent electron transfer. *J. Phys. Chem. B* **2010**, *114*, 14168–14177.

20 Teichen, P. E.; Eaves, J. D. A microscopic model of singlet fission. *J. Phys. Chem. B* **2012**, *116*, 11473–11481.

21 Chan, W.-L.; Ligges, M.; Jailaubekov, A.; Kaake, L.; Miaja-Avila, L.; Zhu, X.-Y. Observing the Multiexciton State in Singlet Fission and Ensuing Ultrafast Multielectron Transfer. *Science* **2011**, *334*, 1541–1545.

22 Chan, W.-L.; Ligges, M.; Zhu, X.-Y. The Energy Barrier in Singlet Fission Can Be Overcome Through Coherent Coupling and Entropic Gain. *Nat. Chem.* **2012**, *4*, 840–845.

23 Kassal, I.; Yuen-Zhou, J.; Rahimi-Keshari, S. Does Coherence Enhance Transport in Photosynthesis? *J. Phys. Chem. Lett.* **2013**, *4*, 362–367.

24 Chan, W.-L.; Tritsch, J. R.; Zhu, X.-Y. Harvesting singlet fission for solar energy conversion: one versus two electron transfer from the quantum mechanical superposition. *J. Am. Chem. Soc.* **2012**, *134*, 18295–18302.

25 Loudon, R. *The quantum theory of light*, 2nd ed.; Clarendon Press: Oxford, 1983; p 39.

26 Provorse, M.; Bao, P.; Chan, W.-L.; Zhu, X.-Y.; Gao, J. Energy and Electronic Coupling in a Quantum Coherent Mechanism for Singlet Fission from Multistate Density Functional Theory. *J. Chem. Phys.* **2013**, *to be submitted*.

27 Berkelbach, T. C.; Hybertsen, M. S.; Reichman, D. R. Microscopic theory of singlet exciton fission. I. General formulation. *J. Chem. Phys.* **2013**, *138*, 114102.

28 Berkelbach, T. C.; Hybertsen, M. S.; Reichman, D. R. Microscopic theory of singlet exciton fission. II. Application to pentacene dimers and the role of superexchange. *J. Chem. Phys.* **2013**, *138*, 114103.

29 Cembran, A.; Song, L.; Mo, Y.; Gao, J. Block-localized density functional theory (BLDFT), diabatic coupling, and its use in valence bond theory for representing reactive potential energy surfaces. *J. Chem. Theory Comput.* **2009**, *5*, 2702–2716.

30 Tersigni, A.; Shi, J.; Jiang, D. T.; Qin, X. R. Structure of tetracene films on hydrogen-passivated Si(001) studied via STM, AFM, and NEXAFS. *Phys. Rev. B* **2006**, *75*, 205326.

31 Perdew, J. P.; Burke, K.; Ernzerhof, M. Generalized gradient approximation made simple. *Phys. Rev. Lett.* **1996**, *77*, 3865–3868.

32 Adamo, C.; Barone, V. Toward Chemical Accuracy in the Computation of NMR Shieldings: the PBE0Model. *Chem. Phys. Lett.* **1998**, *298*, 113–119.

33 Schmidt, M. W.; Baldridge, K. K.; Boatz, J. A.; Elbert, S. T.; Gordon, M. S.; Jensen, J. H.; Koseki, S.; Matsunaga, N.; Nguyen, K. A.; Su, S. J.; Windus, T. L.; Dupuis, M.; Montgomery, J. S. General atomic and molecular electronic structure system. *J. Comput. Chem.* **1993**, *14*, 1347–1363.

34 Yamagata, H.; Norton, J.; Hontz, E.; Olivier, Y.; Beljonne, D.; Brédas, J. L.; Silbey, R. J.; Spano, F. C. The nature of singlet exciton in oligoacene molecular crystals. *J. Chem. Phys.* **2011**, *134*, 204703.

35 Witzel, W. M.; Shabaev, A.; Hellberg, C. S.; Jacobs, V. L.; Efros, A. L. Quantum simulation of multiple-exciton generation in a nanocrystal by a single photon. *Phys. Rev. Lett.* **2010**, *105*, 137401.

36 Troisi, A.; Orlandi, G. Dynamics of the Intermolecular Transfer Integral in Crystalline Organic Semiconductors. *J. Phys. Chem. A* **2006**, *110*, 4065–4070.

37 Redfield, A. G. *Advances in Magnetic Resonance*; Academic Press: New York, 1965.

38 Breuer, H.-P.; Petruccione, F. *The Theory of Open Quantum Systems*; Oxford University Press: Oxford, 2002.